Nanoelectronics and Its New Materials – A NEW ERA OF NANOSCIENCE

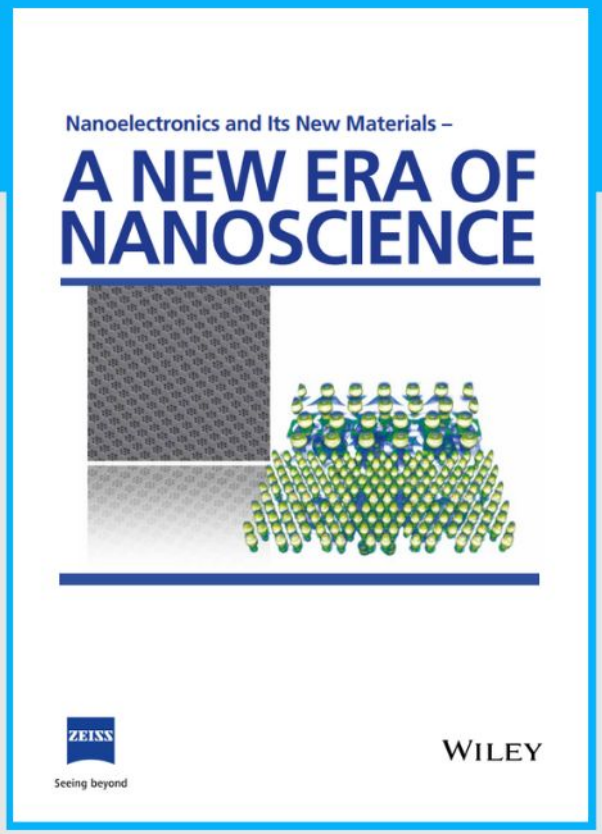

Discover the recent advances in electronics research and fundamental nanoscience.

Nanotechnology has become the driving force behind breakthroughs in engineering, materials science, physics, chemistry, and biological sciences. In this compendium, we delve into a wide range of novel applications that highlight recent advances in electronics research and fundamental nanoscience. From surface analysis and defect detection to tailored optical functionality and transparent nanowire electrodes, this eBook covers key topics that will revolutionize the future of electronics.

To get your hands on this valuable resource and unleash the power of nanotechnology, simply download the eBook now. Stay ahead of the curve and embrace the future of electronics with nanoscience as your guide.

ZEISS

Seeing beyond

WILEY

ADVANCED FUNCTIONAL MATERIALS
www.afm-journal.de

Supramolecular Hydrogel with Orthogonally Responsive R/G/B Fluorophores Enables Multi-Color Switchable Biomimetic Soft Skins

Hao Liu, Shuxin Wei, Huiyu Qiu, Muqing Si, Guoqing Lin, Zhenkuang Lei, Wei Lu, Lei Zhou,* and Tao Chen**

Many living creatures have evolved to show diverse appearance color changes in response to multiple environmental stimuli for attraction, warning, or disguise in their environments. However, it is challenging to construct artificial soft polymer hydrogels with similar multi-responsive multicolor tunable behaviors, but such materials can serve as soft biomimetic skins to dramatically enhance the function of certain machines. Herein, a specially designed material structure to present an innovative class of supramolecular fluorescent polymeric hydrogels with the integrated properties of wide multi-color tunability, multi-responsiveness, self-healing, and remolding capacities is proposed. A key feature of this rational hydrogel design is that multiple fluorophores (blue (B) aggregation-induced emissive and red/green (R/G) lanthanide coordinated ones) are organized separately into different polymer chains of one single supramolecular polymer network. Consequently, the B and R/G fluorophores are engineered to be orthogonally responsive, and the fluorescence intensity of each fluorophore can be controlled independently by different external stimuli, which contribute to multi-responsive multicolor fluorescence response. Besides, the hydrogels also have satisfying self-healing and remolding capacities. All of these promising advantages together further enabled the construction of soft biomimetic color-changing skins that can help the existing robots achieve the desirable camouflaging function.

1. Introduction

Many natural organisms, including octopus, jellyfish, chameleon, and turkey, are found to display the amazing multi-responsive skin color changes (e.g., bio-fluorescent, structural, or pigment color), which are essential survival traits for attraction, warning, and disguise in their environments as a result of natural evolution for tens of thousands of year.[1,2] Inspired by these adaptive colorations in nature, great efforts have now been made to explore various artificial multicolor soft materials for display, camouflage, sensing, and so on.[3–13] Given the high similarity between polymeric hydrogels and animal skins, for example, tissue-like mechanical property and soft wet nature,[14–29] the development of responsive multicolor polymeric hydrogels is attracting great research interest.[30–44] Such materials are not only beneficial to the better understanding of natural color-changing systems, but also capable of serving as soft biomimetic displaying/camouflaging skins to enhance the function of existing actuators/robotics/prosthetics.[45,46] However, compared with structural/pigment color-changing materials, the fluorescent color changeable materials have been very little exploited as soft biomimetic skins, but such systems are very important especially for disguise/display applications in low- or no-light conditions (i.e., night, forest, deep sea).[46] This might be due to the following reasons: 1) the color variation range of most soft fluorescent hydrogels is usually narrow; 2) even if several fluorescent hydrogels with wide multicolor tunability have been reported, they are usually restricted to specific stimulus. They are thus far inferior to those living creatures who can display diverse skin color changes in response to the subtle interplay of multiple environmental changes (e.g., pH, light, temperature, humidity, chemicals).[1,2] In addition, the self-healing feature is also highly desired for long-service durability, while the remolding capacity is helpful to produce materials with various architectures and functions.[47,48] Thus, the fabrication of robust fluorescent hydrogel assemblies with both adaptive multicolor and multi-responsiveness, as well as satisfying self-healing and remolding features, is still highly desired for soft biomimetic skins.

H. Liu, S. Wei, H. Qiu, M. Si, G. Lin, Z. Lei, W. Lu, T. Chen
Key Laboratory of Marine Materials and Related Technologies
Zhejiang Key Laboratory of Marine Materials and Protective Technologies
Ningbo Institute of Materials Technology and Engineering
Chinese Academy of Sciences
Ningbo 315201, China
E-mail: luwei@nimte.ac.cn; tao.chen@nimte.ac.cn
H. Liu, S. Wei, M. Si, Z. Lei, W. Lu, T. Chen
School of Chemical Sciences
University of Chinese Academy of Sciences
19A Yuquan Road, Beijing 100049, China
L. Zhou
National Key Laboratory of Biochemical Engineering
PLA Key Laboratory of Biopharmaceutical Production & Formulation Engineering
Institute of Process Engineering
Chinese Academy of Sciences
Beijing 100190, China
E-mail: zhoulei17@ipe.ac.cn
The ORCID identification number(s) for the author(s) of this article can be found under https://doi.org/10.1002/adfm.202108830.

DOI: 10.1002/adfm.202108830

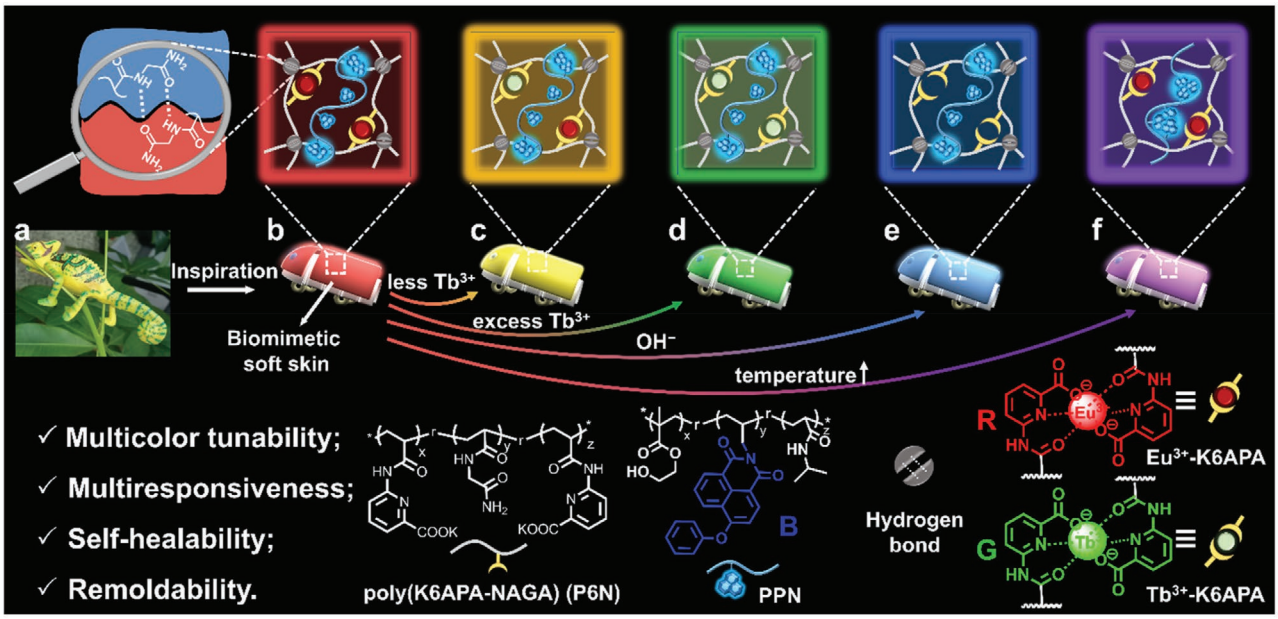

Scheme 1. Schematic illustration showing the material design of the multicolor fluorescent polymer hydrogels, as well as the developed biomimetic soft skins with the adaptive color-changing behavior. a) Photo of a chameleon model. b) Illustration of the red fluorescent hydrogel, which was prepared by delicately organizing the orthogonally responsive aggregation-induced emissive blue fluorogen (B AIE-gen) and Eu^{3+} coordinated red fluorogens (R La-gen) into different polymer chains of one single dynamic polymer network based on supramolecular motifs. Upon exposure to Tb^{3+}, the red fluorescent Eu^{3+}-gens would be transformed into the green fluorescent Tb^{3+}-gens, inducing c) the red-to-yellow or even d) red-to-green color change of the biomimetic hydrogel skin. Moreover, when exposed to the OH^- stimulus, e) the lanthanide coordinated complexes would be decomposed, causing the red-to-blue fluorescence color change. f) Upon environmental temperature elevation, the PPN polymer chain would shrink to induce the heavier aggregation of B AIEgens, resulting in the large enhancement of blue emission and thus red-to-purple fluorescence color change.

This study is seeking an efficient material design to synergistically integrate these above-mentioned features into one single multicolor fluorescent hydrogel system. To do this, two different types of fluorogens, blue aggregation-induced emissive ones (B AIE-gen) and red/green lanthanide coordinated ones (R/G La-gens), are employed and rationally organized into one dynamic polymer network based on supramolecular motifs (**Scheme 1**). On the one hand, the hydrophobic AIE-gens have strong tendency to form intensely fluorescent aggregates in the hydrophilic hydrogel matrix.[49] Any external stimulus, which is capable of inducing the conformational change of polymer chains, can be used to regulate the aggregation extent of AIE-gens, leading to fluorescence color/intensity variation. On the other hand, non-covalent lanthanide coordination is highly dynamic, which will render the hydrogels with potential fluorochromic response to any stimulus that can change the lanthanide-ligand coordination strength of La-gens.[37] More importantly, the B AIE-gen and R/G La-gens are separately introduced into different polymer chains of the supramolecular fluorescent hydrogel. Such a rational polymeric hydrogel structure is highly expected to guarantee the independent and continuous fluorescence intensity regulation of each fluorophore by varying their concentration or using different environmental stimuli (e.g., pH, light, temperature, chemicals). These advantages can contribute synergically to the development of robust chameleon skin-like hydrogel assemblies with multi-responsive multi-color fluorescence tunability. Additionally, the hydrogel materials consisting of dynamic supramolecular polymeric network could be intrinsically self-healable and be processed into soft skin materials with various shapes and architectures.

A proof-of-concept system to demonstrate the proposed design strategy is illustrated in Scheme 1. The substituted naphthalimide, 4-phenoxy-N-allyl-1,8-naphthalimide (PhAN), was chosen as the B AIE-gen,[50] while two La-gens, Eu^{3+}-potassium 6-acrylamidopicolinate (K6APA) and Tb^{3+}-K6APA complexes were employed as the R and G La-gens, respectively.[23] To ensure the distinctly orthogonal responsiveness of these R/G/B luminogens, the B AIE-gen was first covalently introduced into linear thermo-responsive poly(N-isopropyl acrylamide) (PNIPAM), which was then interpenetrated into supramolecular poly(N-acryloyl glycinamide) (PNAGA) network grafted with R and G La-gens. In this rational material design, different-typed fluorogens are organized separately into different polymer chains. This is the key novelty of the present supramolecular fluorescent polymeric hydrogels, in contrast with most reported fluorescent gel systems in which different fluorophores are randomly polymerized into the same cross-linked polymer chains. Owing to the rational organization of these R/G/B luminogens, the fluorescence intensity of each luminogen can be regulated independently and continuously by external environmental stimuli. Consequently, in response to the subtle interplay of several multiple stimuli (temperature, solvent, pH, or light), the fluorescence color of the prepared hydrogels can be programmed easily from red to yellow, green, blue, or purple, nearly covering the full visible spectrum. Additionally, satisfying self-healability and remoldability

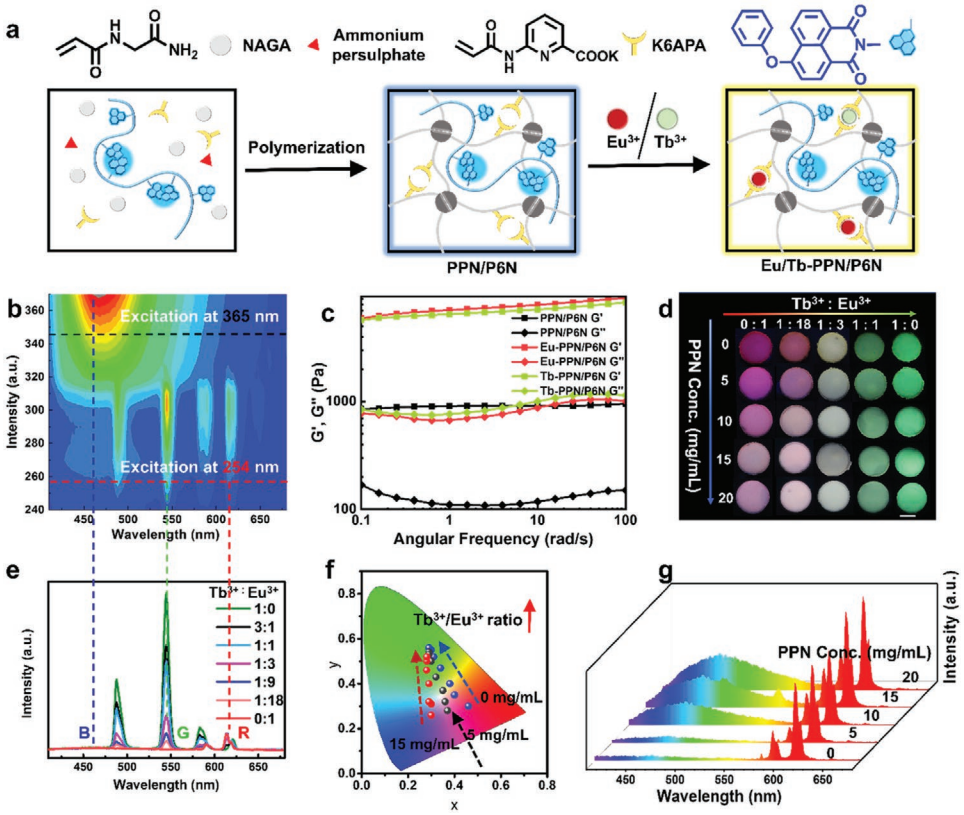

Figure 1. Preparation and characterization of the multicolor fluorescent polymer hydrogels. a) Illustration showing the synthetic procedure of the PPN/P6N and Eu/Tb-PPN/P6N hydrogels. b) Excitation fluorescence mapping of the Eu/Tb-PPN/P6N hydrogel (the Eu^{3+}/Tb^{3+} ratio is 3:1). c) The rheology properties of the PPN/P6N, Eu-PPN/P6N, and Tb-PPN/P6N samples; d) Fluorescent photos of the multicolor fluorescent polymer hydrogels with different Eu/Tb ratios or increasing PPN concentration. These photos were taken under a 254 nm UV lamp. e) Fluorescence spectra of the multicolor fluorescent polymer hydrogels with different Eu/Tb ratios. f) CIE (1931) coordinate diagrams of the multicolor fluorescent polymer hydrogels with different Eu/Tb ratios or increasing PPN concentration. g) Fluorescence spectra of the Eu/Tb-PPN/P6N hydrogel sample with increasing PPN concentration.

were achieved in this non-covalent hydrogel network that is crosslinked by hydrogen bonds and metal coordination interactions. On the basis of these promising properties, we further explored their potential for serving as biomimetic soft skins to help the existing robots achieve dynamic camouflaging function.

2. Results and Discussion

As illustrated in **Figure 1**a, the multicolor fluorescent hydrogels, Eu/Tb-poly(PhAN-NIPAM-HEMA)/poly(K6APA-NAGA) (briefly named as Eu/Tb-PPN/P6N), were prepared by one-step radical polymerization of NAGA[24] and K6APA in the presence of the blue fluorescent poly(PhAN-NIPAM-HEMA) (PPN) polymer (see Table S1, Supporting Information, for the feed formula), followed by the coordination with Eu^{3+} and Tb^{3+} to introduce the green and red emission centers. During the polymerization process, plenty N−H•••O=C hydrogen bonds formed between the pendant amide groups, inducing stable supramolecular crosslinks between the polymer chains. Meanwhile, the linear PPN polymer chains are interpenetrated into the hydrogel matrix by forming vast hydrogen bonds with the newly formed poly(K6APA-NAGA) (P6N) polymer chains, making the blue fluorescent polymer stably and homogeneously distributed in the hydrogel matrix. Subsequently, the red and green fluorescence centers were introduced by coordinating Eu^{3+} and Tb^{3+} with the grafted K6APA moieties to induce the fluorescence enhancement (see the fluorescence spectra in Figure S1, Supporting Information) via the known "antenna effect".[2] Figure 1b shows its excitation-fluorescence spectra, which indicates the simultaneous presence of red (≈614 nm), green (≈544 nm) and blue (≈475 nm) emission bands in this supramolecular hydrogel system. More evidence for the formation of lanthanide-K6APA complexes comes from the rheology measurement, which indicated much higher moduli of Eu/Tb-PPN/P6N than PPN/P6N due to the newly formed lanthanide coordinated crosslinks (Figure 1c). Further studies show that these red, green, and blue fluorescence bands have satisfying photo-luminescent stability at ambient conditions, as is evidenced by the continuous fluorescence spectra recording experiments of Eu-PPN/P6N hydrogel sample (Figure S2, Supporting Information). Furthermore, their photo-luminescent stability could be guaranteed by the fact that these red, green, and blue fluorophores are covalently bonded into the crosslinked polymeric hydrogel network, which indicates that there is no leakage of the bonded fluorophores when responding to external stimuli.

Tunable emission color changes of the Eu/Tb-PPN/P6N hydrogel were then realized by varying either the Tb^{3+}/Eu^{3+} ratios or the concentration of the blue fluorescent PPN polymer (see Table S1, Supporting Information, for the feed formula). As shown in Figure 1d,e, upon raising the Tb^{3+}/Eu^{3+} ratios, the green fluorescence band ≈544 nm gradually increased at the cost of the intensity of the red emission band ≈614 nm. As a result, obvious red-to-green emission color changes were observed (Figure S3, Supporting Information). When increasing the PPN concentration from 0 to 20 mg mL^{-1}, the noticeable red-to-blue color shift was observed (Figure 1d–f and Figure S4a,b, Supporting Information) due to the heavier aggregation of the blue AIEgens, which is evidenced by the large enhancement of blue emission intensity at 475 nm (>8 folds, Figure 1g). Note that only slight blue emission enhancement was observed when raising the PPN concentration from 15 to 20 mg mL^{-1}. This observation probably suggests that the aggregation extent of the AIE-active blue luminogens was large enough to cause remarkable emission enhancement when the PPN concentration is above 15 mg mL^{-1}. Therefore, the supramolecular hydrogel sample containing 15 mg mL^{-1} PPN polymer was optimized as the example for the following studies.

As detailed above, the orthogonally responsive blue AIEgens and red/green La-gens have been specially organized into different polymer chains of the Eu/Tb-PPN/P6N hydrogels. Therefore, it is possible to achieve the remarkable fluorescence color changes by independently regulating the fluorescence intensities of La-gens in response to external stimuli. To demonstrate this, we first examined the fluorochromic response of Eu-PPN/P6N to NaOH, which was known to decompose the red-light-emitting Eu^{3+}-K6APA complexes.[23] **Figure 2**a depicts the time-dependent emission color change of Eu-PPN/P6N in 0.015 M NaOH solutions. The initial red color quickly faded to pink and then blue within several minutes, indicating the gradual decomposition of the Eu^{3+}-K6APA complexes in alkaline solutions. This observation is in agreement with the recorded fluorescence spectra (Figure 2b), which revealed the gradual decrease and finally almost quenching of red emission band, leading to a large increase of the blue/red emission intensity ratio from 0.44 to 5.12 (Figure S5, Supporting Information). It should be noted that only slight intensity change is observed for the blue fluorescence intensity of B AIEgen in response to NaOH stimuli, while the red emission of lanthanide complexes is almost completely quenched. This finding, together with the result obtained in Figure 1g that the red fluorescence intensity of lanthanide complexes is nearly unaffected when increasing the PPN concentration from 0 to 20 mg mL^{-1}, demonstrates that the fluorescence intensities of B AIE-gen and R/G La-gens can be indeed regulated independently. In other words, the B AIE-gen and R/G La-gens are engineered

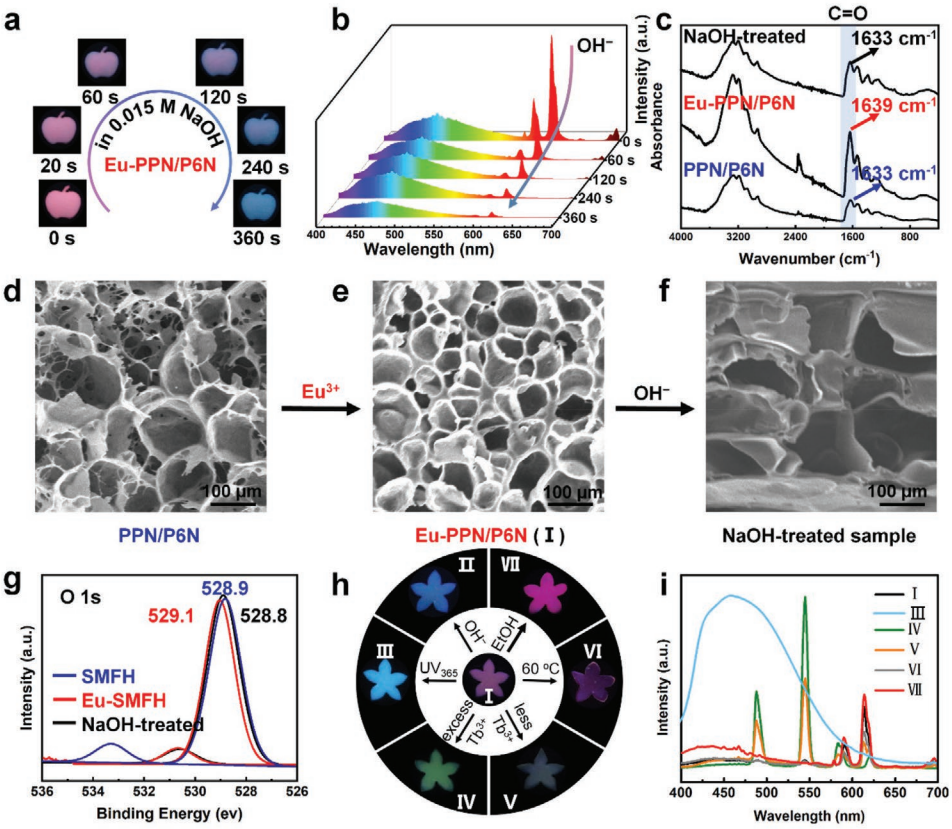

Figure 2. Multi-responsive multi-fluorescence-color tunability of the Eu-PPN/P6N hydrogels. a) Fluorescent photos showing the time dependent color change of Eu-PPN/P6N in 0.015 M NaOH solutions, and b) their corresponding fluorescence spectra. c) ATR-FTIR spectra of the freeze-dried PPN/P6N, Eu-PPN/P6N and the NaOH-treated hydrogel samples, as well as d–f) their SEM images and g) XPS spectra. h) Fluorescent photos showing the multi-color changes of Eu-PPN/P6N in response to multiple environmental changes, and i) their corresponding fluorescence spectra.

to be orthogonally responsive due to the proposed special polymer structure design. Additionally, as expected, retreating the hydrogel with acidic solutions would fully recover its red emission, indicating the reformation of red fluorescent Eu^{3+}-6APA complexes (Figure S6, Supporting Information). To gain more insight into the pH-controlled lanthanide coordination formation and decomposition, several different characterization methods, including Attenuated Total Reflection-Fourier Transform Infrared (ATR-FTIR), X-ray photoelectron spectroscopy (XPS), and scanning electron microscope (SEM) studies, were combined together. As compared in Figure 2c, the characteristic signal of the C=O group shifted to a higher wavenumber (from 1633 to 1639 cm^{-1}) upon Eu^{3+} coordination and then recovered to the initial value after being treated in alkaline solution. Similar signal shift and recovery was also observed in the XPS O 1s spectra (Figure 2g). Consistent with these spectral results, SEM images showed the tightly porous cross-linked network for the red fluorescent Eu-PPN/P6N aerogels (Figure 2e), while much larger pores were noticed for the original PPN/P6N (Figure 2d and Figure S7, Supporting Information) and NaOH-treated samples (Figure 2f). In a similar manner, reversible green-to-blue fluorescence color changes were also demonstrated for Tb-PPN/P6N in response to pH change (Figure S8, Supporting Information). The ATR-FTIR and XPS studies, together with SEM results, clearly demonstrated the pH-controlled lanthanide coordination formation and decomposition.

Besides pH, many other stimuli have also been demonstrated to be capable of regulating the fluorescence intensity of either the blue AIE-gen or Eu^{3+}-K6APA complexes, resulting in multi-responsive emission color changes of Eu-PPN/P6N (Figure 2h,i). For example, when heated to above the lower critical solution temperature (≈32 °C) of PNIPAM, the aggregation extent of blue AIEgens was enhanced by the phase transition of PPN polymer, leading to enhanced blue emission. Meanwhile, there is no obvious change to the red fluorescence band, because the lanthanide-ligand coordination strength of Eu^{3+}-K6APA complexes was nearly unaffected. As a result, red-to-purple fluorescence color change was noticed in response to temperature elevation. Upon exposure to ethanol that can exchange with water to decrease the water content in Eu-PPN/P6N, obvious red fluorescence enhancement was observed due to the reduced hydration effect of Eu^{3+}-K6APA complexes,[14] resulting in much deeper red emission color. Moreover, the addition of Tb^{3+} could react with the red fluorescent Eu^{3+}-K6APA complexes to form the green fluorescent Tb^{3+}-K6APA complexes,[23] leading to the change of red/green intensity ratio. Consequently, red-to-yellow and red-to-green color changes were observed when less or excess amount of Tb^{3+} ions were added, respectively. Last but not the least, the desirable excitation wavelength-dependent fluorescence color change (Ex-Dfc) was also noticed for Eu-PPN/P6N. As shown in Figure 2h, the Eu-PPN/P6N sample glowed red under 254 nm UV illumination, but emitted intense blue light under 365 nm UV illumination. Such a unique Ex-Dfc feature is believed to come from the different excitation energies of the blue AIE-gen and red La-gen. As reported previously by us,[35,50] the blue naphthalimide fluorophore has a strong absorption band ≈365 nm and can thus emit blue light under the excitation of 365 nm (Figure S9, Supporting Information) or higher-energy 254 nm UV light. In contrast, the Eu^{3+}/Tb^{3+}-K6APA complexes can only be excited by higher-energy 254 nm UV light owing to their extremely low absorbance to UV light above 300 nm. All these results clearly highlighted the powerful multicolor fluorescence tunability in response to multiple environmental stimuli, including pH, temperature, solvent, and UV light.

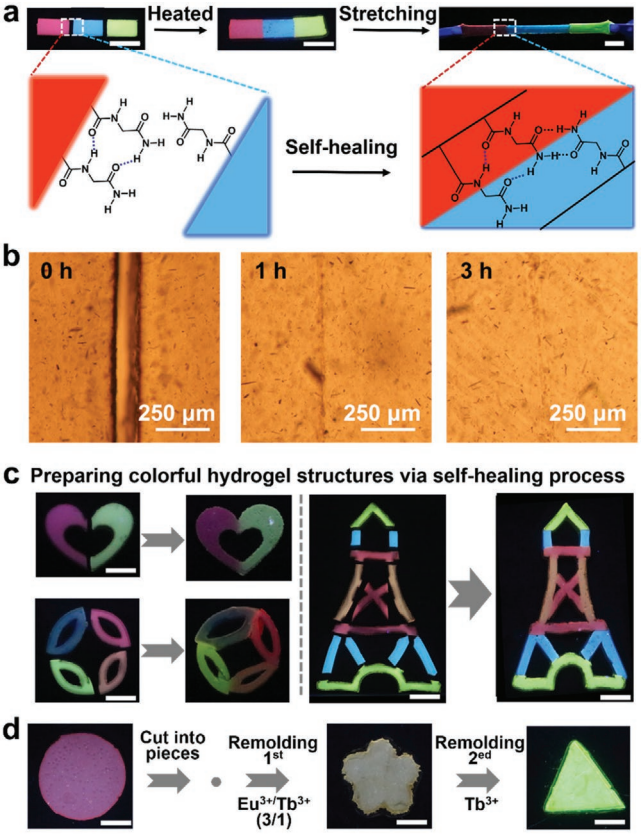

Figure 3. Self-healing and remolding properties. a) Photos showing the self-healing process of the red fluorescent Eu-PPN/P6N, blue fluorescent PPN/P6N and green fluorescent Tb-PPN/P6N hydrogel blocks, as well as the proposed self-healing mechanism. b) Microscopic images of the self-healing process. c) Photos showing the preparation of multicolor fluorescent hydrogel structures via self-healing process. d) Photos showing the reset of both shape and fluorescence color. Scale bar for (a), (c), and (d) is 1 cm.

Other important features of the developed multicolor fluorescent hydrogels include the self-healing and remolding properties, which are endowed by the totally supramolecular crosslinks via dynamic hydrogen bonding and lanthanide coordination interactions.[48] As demonstrated in **Figure 3**a, three distinct fluorescent hydrogel samples (Eu-PPN/P6N, PPN/P6N, and Tb-PPN/P6N) could spontaneously self-heal together to one colorful stretchable hydrogel stripe when heated at 60 °C for a while. Optical images showed the border gradually disappeared and completely vanished within 3 h (Figure 3b). The reshaped hydrogel sample could be stretched to ≈200% while keeping the vivid fluorescence color, indicating the satisfying self-healing stability. Furthermore, more complex hydrogel structures were fabricated to better demonstrate the self-healing property. As shown in Figure 3c, different-shaped Eu/Tb-PPN/P6N hydrogel blocks with diverse emission colors were first tailored by the laser cutting machine and combined together. Benefiting from

the above-described self-healing property, these building blocks could be firmly adhered together to form the integrated object such as a heart, colorful window decoration, Eiffel Tower, and so on (Figures S10–S12, Supporting Information). Additionally, the Eu/Tb-PPN/P6N hydrogels also exhibit satisfying thermoplasticity due to their totally supramolecular crosslinking nature. To demonstrate this, a round-shaped Eu-PPN/P6N hydrogel was cut into pieces and collected in another mold at 80 °C for 3 h. These hydrogel pieces would merge into different new shapes. Especially if Tb^{3+} was added, the reset of both hydrogel shape and color were realized (Figure 3d), which was essential for the following biomimetic color-changing skin use.

The above-described features of Eu/Tb-PPN/P6N hydrogels, including wide multi-color tunability, multi-responsiveness, satisfying self-healing, and remolding abilities, further encouraged us to explore their potential to mimic the biofluorescence color change behaviors of living organisms. For example, treefrogs and butterflies were widely known to have the amazing control over their skin colors and markings in order to match their living environments for predator avoidance. Inspired by this, an artificial hydrogel treefrog with dynamic color-changing function was first designed. As illustrated in **Figure 4**a, its body was prepared from the Eu-PPN/P6N hydrogel. While its skin spots were made from the PPN/PN hydrogel which did not contain the La-gens and thus emitted static blue emission. These body and skin spot hydrogel blocks were then integrated together via self-healing process. As expected, the as-prepared hydrogel treefrog was capable of displaying desirable skin color change in response to environmental stimuli, just behaving like the real-world treefrog (Figure 4b). Similarly, a colorful hydrogel butterfly was also demonstrated by healing different hydrogel blocks together, which could display diverse emission color change accompanying with the environmental change (Figure 4c). It was anticipated that the proposed method will facilitate the fabrication of more complex hydrogel architectures with irregular/curve edges and diverse emission color-changing behaviors, which may find uses as advanced functional materials in various areas such as the soft biomimetic camouflaging robotics.

Besides treefrog and butterflies, many other living creatures (i.e., jellyfish, some spiders) have also evolved to utilize

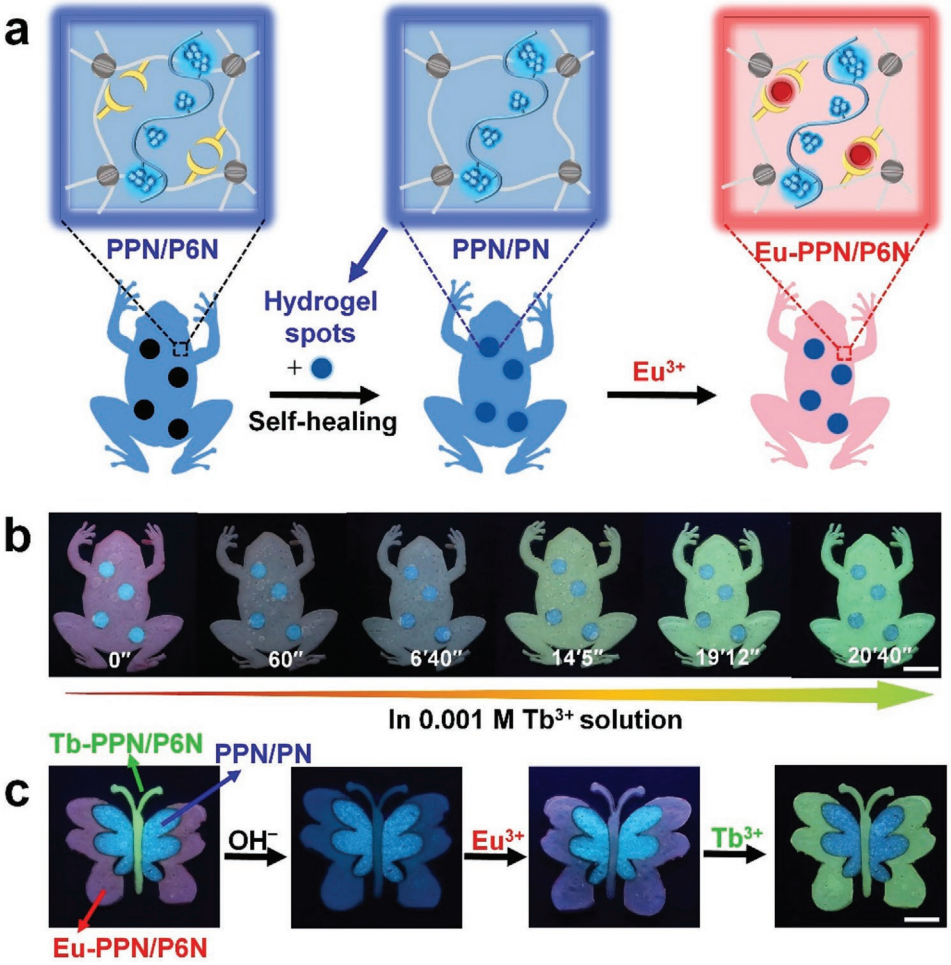

Figure 4. Preparation of the bioinspired hydrogel treefrog and butterfly with adaptive color change behavior. a) Illustration showing the fabrication procedure of the hydrogel treefrog via the self-healing process of different-colored hydrogel blocks. b) Photos showing the adaptive color change of the hydrogel treefrog in aqueous solutions of Tb^{3+}. c) Photos showing the adaptive color change of the hydrogel butterfly in response to different environmental stimuli. Scale bar for (b) and (c) is 1 cm.

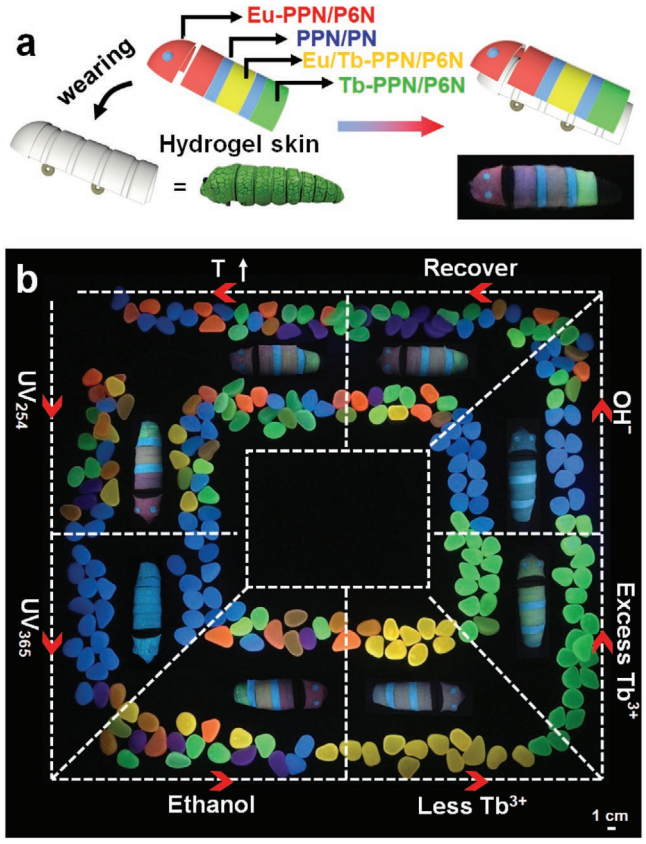

Figure 5. Application of the multicolor fluorescent polymer hydrogels as biomimetic soft skins that can help the robot blend into different-colored background. a) Illustration showing the preparation of the existing robot wearing the biomimetic hydrogel skin, as well as b) the images showing their diverse color change in response to different environmental stimuli. It should be noted that the recovery process means that different parts of the hydrogel skins were further treated by lanthanide ions to recover the initial state.

the responsive biofluorescence color change to achieve the adaptive camouflage functions in their environments. Replication of these natural fluorescence color-changing camouflage behaviors by using soft synthetic hydrogels will be quite promising, because such materials could serve as biomimetic skins to enhance the adaptive camouflaging function of man-made robots. To this end, a conformal biomimetic skin with colorful patterns was constructed through the self-healing process of different-colored hydrogel blocks (**Figure 5**a). As illustrated in Figure 5b, a commercially available caterpillar robot that cannot change its color was employed as the example. Interestingly, after wearing the specially designed multicolor hydrogel skin, a smart robot with adjustable colors and patterns was achieved. At the initial state, the robots displayed four-color fluorescence that can match with the colorful background made of different-colored luminous stones. When the robot moved to a blue-colored background, its hydrogel skin could also be programmed to blue by switching the excited UV light from 254 to 365 nm. Similarly, when the robot moved along the road to different-colored background (e.g., yellow, green), the color of the hydrogel skin could be further programmed to match the background in response to different environmental stimuli such as ethanol, pH, Tb^{3+}, temperature, and so on. This delicately designed experiment has preliminarily demonstrated that our supramolecular fluorescent hydrogel assemblies with multi-responsive multi-color tunability hold the potential to serve as conformal soft skins to help the existing robots achieve the desirable camouflaging function.

3. Conclusion

In summary, we have demonstrated robust supramolecular fluorescent polymeric hydrogels with the integrated features of wide multicolor tunability, multi-responsiveness, self-healing, and remolding abilities, followed by the exploration of their potential use for soft biomimetic skins for the existing robots. These satisfying multi-functions have been proved to stem from the rational material design, that is, the incorporation of orthogonally responsive blue AIE-gen and red/green La-gens into different polymer chains of the supramolecular cross-linked network. On the basis of the synergistic effect of these appealing properties, artificial hydrogel treefrog and butterfly that can behave like their real-world counterparts to show adjustable skin color changes were constructed. Furthermore, the developed hydrogel materials were designed and fabricated as soft biomimetic camouflaging skins, which could be used to help the commercially available robot to blend into different-colored backgrounds in response to different external stimuli (temperature, pH, ions, solvent, and light). This study has made the soft biomimetic color-changing skins accessible and is expected to find potential applications in optical sensing, soft camouflaging robots, visual human–machine interactive technology, and so on. Moreover, the proposed polymer structure design is highly expected to represent an efficient opportunity to finely and rationally organize different fluorogens into one single fluorescent material, which may bring some exciting and even unexpected merits for fluorescent materials.

4. Experimental Section

Materials: N-isopropyl acrylamide (NIPAM, 98.0%), hydroxyethyl methacrylate (HEMA, 98.0%), glycinamide hydrochloride (98.0%), and acryloyl chloride (98.0%) were commercially provided by Tokyo Chemical Industry Co. Ltd. Ammonium persulfate (APS, 98.0%) and N,N,N′,N′-Tetramethylethylenediamine (TEMED, 99.0%) and $Tb(NO_3)_3.5H_2O$ (99.9%) was purchased from Aladdin Chemistry Co., Ltd. $Eu(NO_3)_3.6H_2O$ (99.9%), potassium hydroxide (KOH, 95.0%), and sodium hydroxide (NaOH, 95.0%) were supplied by Energy Chemical. Ether (99.7%) and concentrated HCl (37%) were provided by Sinopharm Chemical Reagent Co., Ltd. Synthetic procedures and the detailed characterization information of NAGA (See its ^{1}H NMR spectrum in Figure S13, Supporting Information), 6APA and PPN have been reported in several previous papers.[24,23,50]

Preparation of the PPN/P6N and PPN/PN Hydrogels: In a typical experiment, NAGA (1 g), APS (10 mg), 6APA (8.2 mg), KOH (2.4 mg), and aqueous solution of PPN (5 mL, 30 mg mL^{-1}) were mixed with 5 mL deionized water. After being completely dissolved, TEMED (23 µL) was added and well-mixed. Finally, the precursor solution was placed into the self-prepared molds with two glass plates and one 0.5 mm thick silicon plate for polymerization at 10 °C for 12 h to produce the PPN/P6N hydrogel. Other PPN/P6N hydrogel samples with different PPN content were prepared by using the feed formula shown in Table S1, Supporting

Information. The PPN/PN hydrogel was prepared by using a similar method, except that the K6APA monomer was not added.

Preparation of the Eu/Tb-PPN/P6N Hydrogels: The as-prepared PPN/P6N hydrogels were first soaked into 0.1 M Eu^{3+} or Tb^{3+} solution for 1 h at room temperature to allow the formation of red and green fluorescent lanthanide complexes. After that, the coordinated hydrogels were immersed into large quantity of deionized water to remove the free lanthanide ions.

Characterization: ^{1}H NMR spectrum of NAGA was recorded on Bruker Advance AMX-400 Spectrometer in D_2O by using tetramethylsilane as the internal reference (Figure S13, Supporting Information). Fluorescence spectra of the hydrogels were measured by Hitachi F-4600 Spectrofluorometer equipped with a xenon (Xe) lamp (150 W). ATR-FT-IR spectra of the freeze-dried hydrogel samples were recorded on a Micro FT-IR (Cary 660+620) instrument. Surface and cross section morphology of the freeze-dried hydrogels were performed by a field-emission SEM (S-4800, Hitachi) with an accelerating voltage of 5.0 kV. Dynamic rheological measurements were characterized by a stress-controlled rheometer (Physica MCR-301, Anton Paar). Images showing the self-healing process were taken by a polarizing microscope (OLYMPUS, 71781687-5). Digital photos of the hydrogels were taken by a canon camera (EOS 750D).

Method to Investigate the pH-Dependent Fluorescence Response of Eu-PPN/P6N Hydrogels: The Eu-PPN/P6N hydrogels were placed into the 0.015 M NaOH solution at room temperature to decompose the lanthanide complexes. The re-formation of lanthanide complexes in the hydrogels were achieved by placing the NaOH-treated sample into the 0.015 M HCl solution. Photos and fluorescence spectra of the samples were then recorded at different time intervals.

Method to Investigate the Self-Healing Property: The as-prepared PPN/P6N, Eu-PPN/P6N, and Tb-PPN/P6N hydrogels were first cut into the hydrogel blocks of different shapes. These building blocks were then brought together to self-heal at 60 °C for 3 h to produce the self-healed hydrogel structures.

Method to Investigate the Remolding Property: The as-prepared Eu-PPN/P6N hydrogels were first cut into pieces and then collected in another glass mold. After being heated at 80 °C for 3 h, these pieces were merged into a new profile.

Method to Prepare the Conformal Hydrogel Skins: As illustrated in Figure 5a, according to the surface sizes of the caterpillar robot, several hydrogel stripes were first cut from the PPN/P6N and PPN/PN hydrogels by using the laser cutting machine. These hydrogel stripes were then combined together and allowed to self-heal together into a conformal hydrogel skin at 60 °C for 3 h. Finally, the multicolor fluorescent hydrogel skin was obtained by spatially spraying the Eu^{3+} solution (0.1 M), Tb^{3+} solution (0.1 M) and Eu^{3+}/Tb^{3+} mixed solution (0.1 M) onto different regions of the hydrogel skin through a self-made polyethylene mask.

Supporting Information

Supporting Information is available from the Wiley Online Library or from the author.

Acknowledgements

H.L. and S.W. contributed equally to this work. This work was supported by the National Natural Science Foundation of China (21774138, 52073297, and 51773215), the Key Research Program of Frontier Sciences, Chinese Academy of Sciences (QYZDB-SSW-SLH036), the National Key Research and Development Program of China (2019YFC1606603), the Youth Innovation Promotion Association of Chinese Academy of Sciences (2019297), and K. C. Wong Education Foundation (GJTD-2019-13).

Conflict of Interest

The authors declare no conflict of interest.

Data Availability Statement

Research data are not shared.

Keywords

aggregation-induced emission, biomimetic skins, dynamic polymer networks, lanthanide coordination, supramolecular fluorescent hydrogels

Received: September 1, 2021
Revised: October 13, 2021
Published online: November 18, 2021

[1] E. A. Widder, *Science* **2010**, *328*, 704.
[2] S. Wei, Z. Li, W. Lu, H. Liu, J. Zhang, T. Chen, B. Z. Tang, *Angew. Chem., Int. Ed.* **2021**, *60*, 8608.
[3] B. B. Patel, D. J. Walsh, D. H. Kim, J. Kwok, B. Lee, D. Guironnet, Y. Diao, *Sci. Adv.* **2020**, *6*, eaaz7202.
[4] H. H. Chou, A. Nguyen, A. Chortos, J. W. To, C. Lu, J. Mei, T. Kurosawa, W. G. Bae, J. B. Tok, Z. Bao, *Nat. Commun.* **2015**, *6*, 8011.
[5] J. Mu, G. Wang, H. Yan, H. Li, X. Wang, E. Gao, C. Hou, A. T. C. Pham, L. Wu, Q. Zhang, Y. Li, Z. Xu, Y. Guo, E. Reichmanis, H. Wang, M. Zhu, *Nat. Commun.* **2018**, *9*, 590.
[6] Y. Liu, C. Shao, Y. Wang, L. Sun, Y. Zhao, *Matter* **2019**, *1*, 1581.
[7] A. Lavrenova, D. W. Balkenende, Y. Sagara, S. Schrettl, Y. C. Simon, C. Weder, *J. Am. Chem. Soc.* **2017**, *139*, 4302.
[8] Y. Yao, C. Yin, S. Hong, H. Chen, Q. Shi, J. Wang, X. Lu, N. Zhou, *Chem. Mater.* **2020**, *32*, 8868.
[9] J. M. Clough, J. Gucht, T. E. Kodger, J. Sprakel, *Adv. Funct. Mater.* **2020**, *30*, 2002716.
[10] D. Kim, J. E. Kwon, S. Y. Park, *Adv. Funct. Mater.* **2018**, *28*, 1706213.
[11] H. Tan, Q. Lyu, Z. Xie, M. Li, K. Wang, K. Wang, B. Xiong, L. Zhang, J. Zhu, *Adv. Mater.* **2019**, *31*, 1805496.
[12] G. Isapour, M. Lattuada, *Adv. Mater.* **2018**, *30*, 1707069.
[13] X. Ji, B. Shi, H. Wang, D. Xia, K. Jie, Z. L. Wu, F. Huang, *Adv. Mater.* **2015**, *27*, 8062.
[14] W. Lu, M. Si, H. Liu, H. Qiu, S. Wei, B. Wu, R. Wang, G. Yin, J. Zhang, P. Theato, Y. Wei, T. Chen, *Cell Rep. Phys. Sci.* **2021**, *2*, 100417.
[15] T. Wu, T. Yin, X. Hu, G. Nian, S. Qu, W. Yang, *Adv. Opt. Mater.* **2020**, *8*, 2000031.
[16] S. Wei, H. Qiu, H. Shi, W. Lu, H. Liu, H. Yan, D. Zhang, J. Zhang, P. Theato, Y. Wei, T. Chen, *ACS Nano* **2021**, *15*, 10415.
[17] Q. M. Zhang, W. Xu, M. J. Serpe, *Angew. Chem., Int. Ed.* **2014**, *53*, 4827.
[18] L. Hu, Y. Wan, Q. Zhang, M. J. Serpe, *Adv. Funct. Mater.* **2020**, *30*, 1903471.
[19] K. Sano, Y. Ishida, T. Aida, *Angew. Chem., Int. Ed.* **2018**, *57*, 2532.
[20] G. Stoychev, C. Reuther, S. Diez, L. Ionov, *Angew. Chem., Int. Ed.* **2016**, *55*, 16106.
[21] W. Lu, X. X. Le, J. W. Zhang, Y. J. Huang, T. Chen, *Chem. Soc. Rev.* **2017**, *46*, 1284.
[22] C. Lowenberg, M. Balk, C. Wischke, M. Behl, A. Lendlein, *Acc. Chem. Res.* **2017**, *50*, 723.
[23] S. X. Wei, W. Lu, X. X. Le, C. X. Ma, H. Lin, B. Y. Wu, J. W. Zhang, P. Theato, T. Chen, *Angew. Chem., Int. Ed.* **2019**, *58*, 16243.
[24] X. Y. Dai, Y. Y. Zhang, L. N. Gao, T. Bai, W. Wang, Y. L. Cui, W. G. Liu, *Adv. Mater.* **2015**, *27*, 3566.
[25] H. Yuk, S. T. Lin, C. Ma, M. Takaffoli, N. X. Fang, X. H. Zhao, *Nat. Commun.* **2017**, *8*, 14230.

[26] J. Kim, J. A. Hanna, M. Byun, C. D. Santangelo, R. C. Hayward, *Science* **2012**, *335*, 1201.
[27] T. Matsuda, R. Kawakami, R. Namba, T. Nakajima, J. P. Gong, *Science* **2019**, *363*, 504.
[28] Y. F. Ma, M. T. Hua, S. W. Wu, Y. J. Du, X. W. Pei, X. Y. Zhu, F. Zhou, X. M. He, *Sci. Adv.* **2020**, *6*, eabd2520.
[29] W. X. Fan, C. Y. Shan, H. Y. Guo, J. W. Sang, R. Wang, R. R. Zheng, K. Y. Sui, Z. H. Nie, *Sci. Adv.* **2019**, *5*, eaav7174.
[30] J. Wang, S. Sun, B. Wu, L. Hou, P. Ding, X. Guo, M. A. Cohen Stuart, J. Wang, *Macromolecules* **2019**, *52*, 8643.
[31] Z. Li, G. Wang, Y. Wang, H. Li, *Angew. Chem., Int. Ed.* **2018**, *57*, 2194.
[32] J. Wang, F. Tang, Y. Wang, S. Liu, L. Li, *Adv. Opt. Mater.* **2020**, *8*, 1901571.
[33] H. Chen, F. Y. Yang, Q. Chen, J. Zheng, *Adv. Mater.* **2017**, *29*, 1606900.
[34] Q. D. Zhu, K. Van Vliet, N. Holten-Andersen, A. Miserez, *Adv. Funct. Mater.* **2019**, *29*, 1808191.
[35] Y. Zhang, X. Le, Y. Jian, W. Lu, J. Zhang, T. Chen, *Adv. Funct. Mater.* **2019**, *29*, 1905514.
[36] D. Lu, M. Zhu, S. Wu, Q. Lian, W. Wang, D. Adlam, J. A. Hoyland, B. R. Saunders, *Adv. Funct. Mater.* **2020**, *30*, 1909359.
[37] G. Weng, S. Thanneeru, J. He, *Adv. Mater.* **2018**, *30*, 1706526.
[38] X. Ji, R. T. Wu, L. Long, X. S. Ke, C. Guo, Y. J. Ghang, V. M. Lynch, F. Huang, J. L. Sessler, *Adv. Mater.* **2018**, *30*, 1705480.
[39] X. Ji, Z. Li, X. Liu, H. Q. Peng, F. Song, J. Qi, J. W. Y. Lam, L. Long, J. L. Sessler, B. Z. Tang, *Adv. Mater.* **2019**, *31*, 1902365.
[40] Y. Zhang, Y. Chen, J. J. Li, L. Liang, Y. Liu, *Acta Chim. Sin.* **2018**, *76*, 622.
[41] C. N. Zhu, T. Bai, H. Wang, W. Bai, J. Ling, J. Z. Sun, F. Huang, Z. L. Wu, Q. Zheng, *ACS Appl. Mater. Interfaces* **2018**, *10*, 39343.
[42] C. N. Zhu, T. Bai, H. Wang, J. Ling, F. Huang, W. Hong, Q. Zheng, Z. L. Wu, *Adv. Mater.* **2021**, *33*, 2102023.
[43] Q. Ma, M. Zhang, C. Yao, Y. Du, D. Yang, *Chem. Eng. J.* **2020**, *394*, 124894.
[44] D. Li, W. Hu, J. Wang, Q. Zhang, X. M. Cao, X. Ma, H. Tian, *Chem. Sci.* **2018**, *9*, 5709.
[45] J. H. Pikul, S. Li, H. Bai, R. T. Hanlon, I. Cohen, R. F. Shepherd, *Science* **2017**, *358*, 210.
[46] S. A. Morin, R. F. Shepherd, S. W. Kwok, A. A. Stokes, A. Nemiroski, G. M. Whitesides, *Science* **2012**, *337*, 828.
[47] D. L. Taylor, M. I. H. Panhuis, *Adv. Mater.* **2016**, *28*, 9060.
[48] M.-X. Li, M.-Z. Rong, M.-Q. Zhang, *Chin. J. Polym. Sci.* **2020**, *39*, 545.
[49] W. Lu, S. Wei, H. Shi, X. Le, G. Yin, T. Chen, *Aggregate* **2021**, *2*, e37.
[50] H. Liu, S. X. Wei, H. Y. Qiu, B. B. Zhan, Q. Q. Liu, W. Lu, J. W. Zhang, O. Ngai, T. Chen, *Macromol. Rapid Commun.* **2020**, *41*, 2000123.